Anisotropic Spin Relaxation in Graphene

N. Tombros,[1] S. Tanabe,[1] A. Veligura,[1] C. Jozsa,[1] M. Popinciuc,[2] H. T. Jonkman,[2] and B. J. van Wees[1]

[1]*Physics of Nanodevices, Nijenborgh 4, 9747 AG Groningen, The Netherlands*

[2]*Molecular Electronics, Zernike Institute for Advanced Materials, Rijksuniversiteit Groningen, Nijenborgh 4, 9747 AG Groningen, The Netherlands*

(Received 20 February 2008; published 25 July 2008)

Spin relaxation in graphene is investigated in electrical graphene spin valve devices in the nonlocal geometry. Ferromagnetic electrodes with in-plane magnetizations inject spins parallel to the graphene layer. They are subject to Hanle spin precession under a magnetic field B applied perpendicular to the graphene layer. Fields above 1.5 T force the magnetization direction of the ferromagnetic contacts to align to the field, allowing injection of spins perpendicular to the graphene plane. A comparison of the spin signals at $B = 0$ and $B = 2$ T shows a 20% decrease in spin relaxation time for spins perpendicular to the graphene layer compared to spins parallel to the layer. We analyze the results in terms of the different strengths of the spin-orbit effective fields in the in-plane and out-of-plane directions and discuss the role of the Elliott-Yafet and Dyakonov-Perel mechanisms for spin relaxation.

DOI: 10.1103/PhysRevLett.101.046601 PACS numbers: 72.25.Rb, 72.25.Hg, 73.63.−b

The discovery of the anomalous quantum Hall effect in graphene [1,2] triggered an avalanche of theoretical and experimental work on this new system. Spintronics is one of the fields which has great expectations for this material. Spin qubits [3] and many other spintronic devices based on graphene could become available due to the fact that in intrinsic graphene spins are expected to relax very slowly [4–7]. The reason behind this is the low hyperfine interaction of the spins with the carbon nuclei (only 1% of the nuclei are ^{13}C and have spin) and the weak spin-orbit (SO) interaction due to the low atomic number.

Recent experiments show spin transport in graphene up to room temperature [8–13], with spin relaxation lengths of 2 μm and relaxation times around 150 ps [8]. Such relatively short relaxation times suggest an important role of SO interaction. There are two relevant mechanisms for SO interaction in graphene [14]. In the Elliott-Yafet (EY) mechanism, spin scattering is induced by electron (momentum) scattering from impurities, boundaries and phonons. The Dyakonov-Perel (DP) mechanism results from SO terms in the Hamiltonian of the clean material. Here electrons feel an effective magnetic field, which changes in direction every time the electron scatters to a different momentum state, resulting in random spin precession. In principle the two mechanisms can be distinguished by their different dependence on the momentum scattering time τ [14]. In our experiments in graphene we are not able to change τ considerably, making the distinction between both mechanisms difficult. However, we can obtain valuable information about the SO interaction by investigating the anisotropy of spin relaxation. First we note that the transverse (T_2) and longitudinal (T_1) spin relaxation times are expected to be the same for the parameters of our system [14]. Therefore, as in metals, a single spin relaxation time $T = T_1 = T_2$ can be used. However, due to the two-dimensionality, T can have a different value for injected spins parallel ($T_\parallel$) or perpendicular ($T_\perp$) to the graphene plane. For example, if the SO interaction is of the Rashba or Dresselhaus type then the SO effective fields are exclusively in the graphene plane and calculations show that this should result in anisotropic spin relaxation in which $T_\perp = \frac{1}{2}T_\parallel$ [14]. On the other hand, if the SO effective fields pointing out of the graphene plane dominate, we expect $T_\perp \gg T_\parallel$.

Our experiments are performed using the four terminal ''nonlocal'' technique [Fig. 1(a)]. Here the charge current path can be fully separated from the voltage detection circuit [15]. The nonlocal technique is less sensitive to device resistance fluctuations and magnetoresistances (such as Hall effects), as compared to the standard two-terminal spin valve technique. This allows the detection of small spin signals, in our case as small as a few mΩ [Fig. 2(a)]. Fabrication of the devices is done as in Ref. [8]. Using the ''Scotch tape'' technique [16] graphene layers were deposited on an oxidized (500 nm) heavily doped Si wafer. Calibrations by Raman spectroscopy in combination with optical microscopy and atomic force microscopy show that our samples are single graphene layers. We evaporate a thin layer of aluminum (6 Å) on top of the graphene layer at 77 K and let it oxidize using pure O_2, to form an Al_2O_3 barrier. These barriers very likely contain pinholes [8], nevertheless spin injection efficiencies of 10% have been observed. Conventional electron beam lithography and e-beam evaporation of 50 nm of Co (at 10^{-6} mbar) are used to define the ferromagnetic cobalt electrodes. The electrodes have different widths to assure different switching fields [15]. The experiments are performed at a temperature of 4.2 K and we use magnetic fields up to 4.5 T. A standard ac lock-in technique is used with currents in the range 1–20 μA.

Spin precession measurements are performed on two samples (graphene width $W = 1.2$ μm) for electrode spacings $L = 5$ μm (sample A), 0.5, 2, and 4 μm (sample B). To perform the Hanle spin precession experiments we first

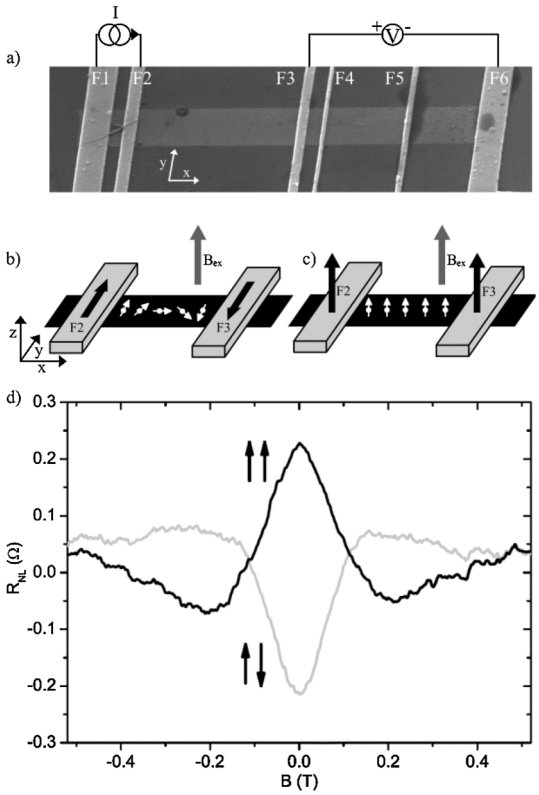

FIG. 1. Spin transport in graphene. (a) A SEM picture of a single layer of graphene contacted by 6 cobalt electrodes (sample A). Spins traveling a distance of 5 μm, from cobalt electrode $F2$ to $F3$, are probed using the nonlocal geometry. The voltage circuit ($F3$-graphene- $F6$) is completely separated from the current circuit ($F1$-graphene- $F2$). (b) Hanle type spin precession experiment, the magnetization of the spin injector $F2$ is set antiparallel to the magnetization of spin detector $F3$. Spins are injected parallel to the graphene plane. (c) Application of a strong external magnetic field (~1.4 T) perpendicular to the graphene layer results in injector and detector magnetizations aligned parallel to the external magnetic field. Spins are injected perpendicular to the graphene plane. (d) Hanle spin precession in case of parallel (↑↑, black curve) and antiparallel (↑↓, gray curve) magnetizations.

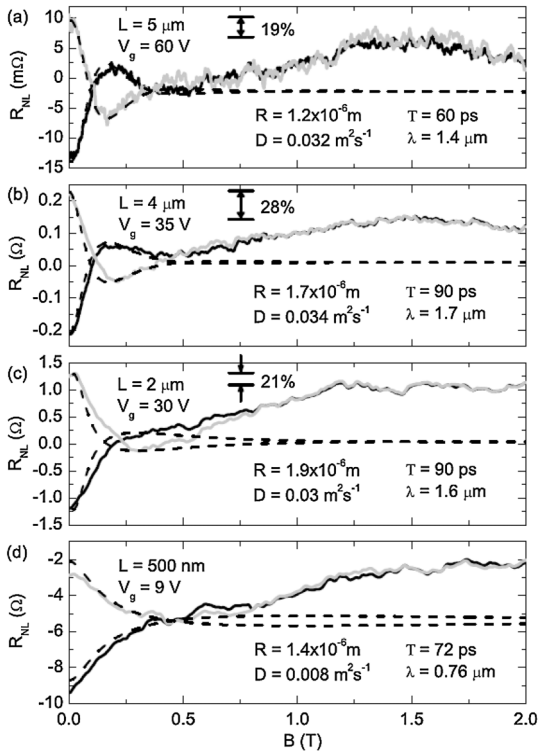

FIG. 2. Anisotropic spin relaxation at high electron density n (a) $n = 2.1 \times 10^{12}$ cm^{-2}. Initially, spins are injected parallel to the graphene plane having the magnetization of the spin injector set parallel (gray line) or antiparallel (black line) to the detector (at a distance $L = 5$ μm). From the fits (dashed line) we extract the diffusion constant D and the relaxation time $T_{\|}$. A magnetic field of ~1.4 T is needed to align the magnetization of the cobalt electrodes out of their easy magnetization axis, in this case the spins are injected perpendicular to the graphene layer having a spin relaxation time $T_{\perp}$. $T_{\perp}$ is 19% smaller to $T_{\|}$. The small decrease in the nonlocal signal found between 1.5 and 2 T is attributed to a background due to orbital magnetoresistance effects. The same experiment has been performed on sample B for (b) $L = 4$ μm ($n = 3.5 \times 10^{12}$ cm^{-2}), (c) $L = 2$ μm ($n = 2.8 \times 10^{12}$ cm^{-2}) and (d) $L = 500$ nm ($n = 3.5 \times 10^{12}$ cm^{-2}).

apply a magnetic field in the y direction to prepare the magnetizations of the electrodes in a parallel or antiparallel orientation [Fig. 1(a)]. Then this field is removed and a B field in the z direction is scanned [Fig. 1(b)] [15]. An example of the resulting spin precession is depicted in Fig. 1(d) (sample B), for the parallel and antiparallel magnetizations of the spin injector and spin detector cobalt electrodes. The spins are injected parallel to the graphene plane and are precessing while diffusing towards the spin detector situated at a distance $L = 4$ μm from the injector. At $B_z \sim 0.2$ T the average precession angle is 180 degrees, resulting in a sign reversal of the spin signal. The magnitude of the signal at $B_z = 0$ T (0.2 Ω) is small compared to the signals measured in our previous work, which was in the order of 2 Ω for these spacings [8]. This is directly related to the measured low contact resistances R_c (1–2 kΩ), which are a factor 5 to 10 smaller than in Ref. [8]. In this study, the contact resistance R_c is equal or smaller to the typical square resistance of the graphene layer R_{sq} and this results in the reduction of the injection/detection efficiencies and also provides an extra path for spin relaxation at the ferromagnetic contacts [17]. This is taken into account in the fitting of the spin precession measurements with solutions of the one-dimensional Bloch equations which describe the combined effect of diffusion, precession, and spin relaxation in the system:

$$D\frac{d^2\vec{\mu}}{dx^2} - \frac{\vec{\mu}}{T} + \frac{g\mu_B}{\hbar}(\vec{B} \times \vec{\mu}) = 0, \qquad (1)$$

where D is the diffusion constant, μ is spin accumulation, T is the spin relaxation time, g is the g factor ($g \approx 2$), B the magnetic field, $\hbar$ is Planck's constant and μ_B the Bohr magneton. From the fit, the spin relaxation time T in

graphene can be extracted. In our model we assume a spin injector electrode at position $x = 0$ and a spin detector electrode at position $x = L$. The additional spin relaxation due to the finite contact resistance R_c is taken into account by a parameter $R = WR_c/R_{sq}$, where W is the width of the graphene layer. If the spin relaxation length is in the μm range then the model shows that for $R \gg 10^{-5}$ m the contacts do not induce extra spin relaxation. On the other hand, for $R \ll 10^{-5}$ m the amplitude (A) of the spin signal has a quadratic dependence on R ($A \sim R^2$) [18].

We start by applying a gate voltage on samples A and B to allow us to investigate the spin dynamics at a high electron density $n_e \sim 3.0 \times 10^{16}$ m^{-2} (Fig. 2). From the fitting procedure both the diffusion constant D and the spin relaxation time $T_\parallel$ can be obtained. For $L = 2$, 4 (sample B) and 5 μm (sample A) we obtain a diffusion constant of 3×10^{-2} m^2 s^{-1} and spin relaxation times of $T_\parallel = 60$ ps for sample A up to 90 ps for sample B, corresponding to spin relaxation lengths $\lambda = \sqrt{DT_\parallel}$ of 1.4 up to 1.8 μm, respectively, comparable to the values found in Ref. [8]. Increasing the magnitude of B_z results in a rotation of the magnetization of the cobalt electrodes out of the plane, towards the magnetic field direction. This can already be seen in Fig. 1(d) where the rotation of the magnetization induces an asymmetry of the spin signal at 0.5 T. A magnetic field of 1.4 to 1.8 T is needed to fully align the magnetization of the cobalt electrodes in the z direction [Fig. 1(c)] [15,19]. The injected spins are now perpendicular to the graphene layer and will relax with a time $T_\perp$ which is not necessarily the same as $T_\parallel$. If the anisotropy in the spin relaxation is large then the amplitude of the nonlocal spin signal at $B = 0$ T should be very different from the signal at $\sim$1.8 T. In Fig. 2 the decrease in the magnitude of the spin signal for $L = 2$, 4 and 5 μm corresponds to a spin relaxation time $T_\perp$ being 20% smaller than $T_\parallel$. Clearly, our devices show anisotropic spin relaxation in graphene at high electron densities. Of interest is to investigate if the same conclusion holds for spins injected in graphene at the charge neutrality point. For $L = 2$, 4, and 5 μm, close to the Dirac point, orbital magnetoresistance effects induce a large background, increasing quadratically in B_z. This background is not only monotonic increasing, it also contains nonperiodic fluctuations as a function of B_z with an amplitude equal or larger than the spin signal. This effect, in combination with the large suppression of the spin signal amplitude at the Dirac point, for $L = 2$, 4, and 5 μm, does not allow us to investigate in precision the spin anisotropy. However, we were able to perform the experiment for the $L = 0.5$ μm spacing in which the spin signal is relatively large. [Fig. 3(c)] Here, application of a gate voltage of -76.5 V [Fig. 3(a)] allows us to investigate the spin dynamics at the Dirac point. Clearly, the nonlocal resistance at 2T is smaller than the resistance at $B_z = 0$ T showing similar anisotropic spin relaxation behavior as for high electron densities.

We can now estimate the effective magnetic field which the electrons feel, assuming the Dyakonov-Perel mechanism. The electron scatters to a different momentum state after a time τ which results in a precession angle of the spin $\Delta\omega = \omega_p\tau$. Here, ω_p is the precession frequency of the spin. The number of scattering events necessary to induce an angle of 2π is $\sqrt{T/\tau}$. Using $T = 100$ ps and $\tau \sim 30$ fs we obtain $\omega_p \sim 10^{12}$ s^{-1}. Therefore, in the Dyakonov-Perel mechanism, the precession frequency corresponds to an effective magnetic field of about 5 T.

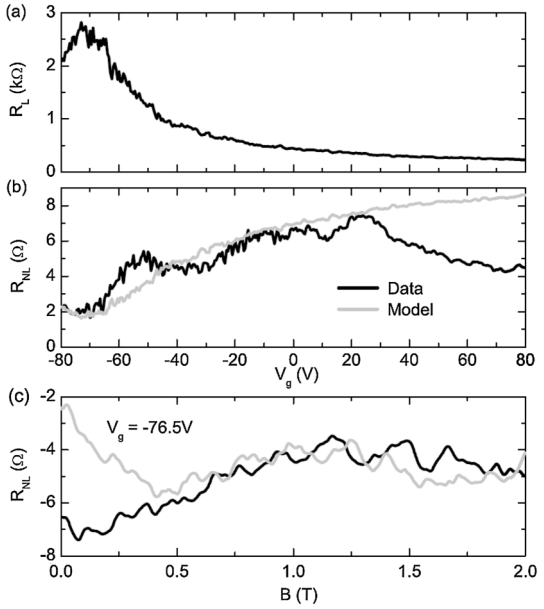

FIG. 3. Anisotropic spin relaxation at the Dirac point for $L = 500$ nm (a) Gate voltage dependence of the graphene resistance between electrodes F_2 and F_3 [Fig. 1(a)]. The charge neutrality point is found at $Vg \approx -75$ V. (b) The nonlocal resistance for spins injected parallel to the graphene layer (black line). This is defined as the difference in the signal obtained for injector and detector magnetizations set parallel ($R_{NL,\uparrow\uparrow}$) and the signal for injector and detector set to antiparallel ($R_{NL,\uparrow\downarrow}$). Our model (gray line) which takes into account the finite contact resistance gives a qualitatively good fit to the data for $V_g < 30$ V. (c) Hanle spin precession at the Dirac point (see Fig. 2 and text).

We now check if the transverse (T_2) and longitudinal (T_1) relaxation times for spins in the graphene plane are the same. For this, λ ($=\sqrt{DT_1}$) is extracted from the spin signal dependence on L (Fig. 4). Care has to be given to the strong suppression of the spin signal amplitude as we approach the Dirac point, found at 4.2 K and as well at room temperature. Our model takes into account the spin relaxation at the contacts and fits qualitatively well the data [Fig. 3(b)]. Earlier work did not show this strong effect due to the fact that in those samples the contact resistances were large enough to not to influence the spin dynamics. In Fig. 4 we present the amplitude of the spin signal of sample B as function of the electrode spacing L (= 0.5, 2, and 4 μm) for different values of R. In the same figure we present the length dependence in the signal expected from our model. At high electron densities n [Fig. 4(a)] the model gives a spin relaxation length of 1.5 ± 0.2 μm.

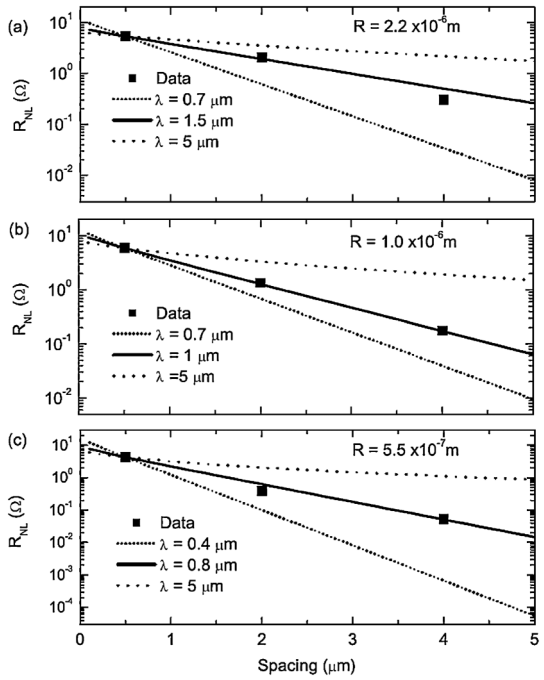

FIG. 4. Dependence of the spin signal as function of electrode spacing L for spins injected parallel to the graphene plane. (a) The gate voltage V_g is set in such a way that for $L = 0.5$, 2 and 4 μm we have the same value of $R = 2.2 \times 10^{-6}$ m ($n \simeq 5.0 \times 10^{12}$ cm^{-2}, $D = 0.04$ m^2 s^{-1}). We obtain a relaxation length of $\lambda = 1.5 \pm 0.2$ μm which is similar to the length extracted from the spin precession measurements (see Fig. 2). Model calculations for $\lambda = 0.7$ μm and $\lambda = 5$ μm are shown for comparison. (b) Moving towards the Dirac point using a gate voltage in such a way that we decrease the R value to 1.0×10^{-6} m ($n \simeq 2 \times 10^{12}$ cm^{-2}, $D = 0.03$ m^2 s^{-1}) has a strong influence in λ, as it decreases to 1 μm and (c) to 0.8 μm (for $R = 5.5 \times 10^{-7}$ m, $n \simeq 1.0 \times 10^{12}$ cm^{-2}, $D = 0.02$ m^2 s^{-1}).

This value is comparable to the values found from spin precession measurements (Fig. 2) performed at similar values of n (and R), proving that $T_1 \simeq T_2$. The effect on λ when we approach the Dirac point is stronger: our model gives $\lambda = 1$ μm for $n \simeq 2.0 \times 10^{12}$ cm^{-2} [Fig. 4(b)] and $\lambda = 0.8$ μm for $n \simeq 1.0 \times 10^{12}$ cm^{-2} [Fig. 4(c)]. Interestingly, the diffusion constant D, obtained from conductivity measurements, is a factor 2 smaller close to the Dirac point [Fig. 4(c)] compared to the value found at high electron density [Fig. 4(a)]. Since $\lambda = \sqrt{DT_1}$ and $D = 1/2v_F^2\tau$ (v_F: Fermi velocity, τ: electron momentum scattering time) this supports the Elliot-Yafet mechanism, where $T_1 \propto \tau$.

Summarizing, we observe that $T_\perp$ is almost 20% smaller than $T_\parallel$ [20]. This anisotropy is expected for a 2D system where spin-orbit fields in plane dominate the spin relaxation. However, the large value for the SO fields (5T) required to describe the result in the Dyakonov-Perel mechanism, combined with the observed dependence of the spin relaxation length λ on the electron momentum scattering time τ suggest that the dominating mechanism is the Elliott-Yafet mechanism. Note that in principle the EY mechanism can also give rise to anisotropic spin relaxation due to the two-dimensional nature of the graphene. As a next step we suggest investigating the dependence of $T_\perp$ and $T_\parallel$ on graphene mobility. An increase in mobility by a factor 10 [21] corresponds to a tenfold increase in τ which would unambiguously show the relative importance of the Elliott-Yafet mechanism compared to the Dyakonov-Perel mechanism.

We thank Bernard Wolfs, Siemon Bakker, Thorsten Last for technical assistance and for useful discussions. This work was financed by MSC^{plus}, NanoNed, NWO (via a "PIONIER" grant) and FOM (via the "Graphene-based electronics" program). The work of Shinichi Tanabe was supported by Osaka University.

[1] Novoselov *et al.*, Nature (London) **438**, 197 (2005).
[2] Zhang *et al.*, Nature (London) **438**, 201 (2005).
[3] B. Trauzettel, D. V. Bulaev, D. Loss, and G. Burkard, Nature Phys. **3**, 192 (2007).
[4] C. L. Kane and E. J. Mele, Phys. Rev. Lett. **95** 226801 (2005).
[5] D. Huertas Hernando, F. Guinea, and A. Brataas, Phys. Rev. B **74**, 155426 (2006).
[6] Y. Yao *et al.*, arXiv:0606.3503.
[7] Honki Min *et al.*, Phys. Rev. B **74**, 165310 (2006).
[8] N. Tombros *et al.*, Nature (London) **448**, 571 (2007).
[9] E. W. Hill, A. K. Geim, K. Novoselov, F. Schedin, and P. Blake, IEEE Trans. Magn. **42**, 2694 (2006).
[10] S. Cho, Y. F. Chen, and M. S. Fuhrer, Appl. Phys. Lett. **91**, 123105 (2007).
[11] M. Nishioka and A. M. Goldman, Appl. Phys. Lett. **90**, 252505 (2007).
[12] M. Ohishi *et al.*, Jpn. J. Appl. Phys. **46**, L605 (2007).
[13] W. H. Wang, K. Pi, Y. Li, Y. F. Chiang, P. Wei, J. Shi, and R. K. Kawakami, Phys. Rev. B **77**, 020402(R) (2008).
[14] J. Fabian, A. Matos-Abiague, C. Ertler, P. Stano, and I. Zutic, arXiv:0711.1461.
[15] F. J. Jedema *et al.*, Nature (London) **416**, 713 (2002).
[16] A. K. Geim and K. S. Novoselov, Nat. Mater. **6**, 183 (2007).
[17] G. Schmidt, D. Ferrand, L. W. Molenkamp, A. T. Filip, and B. J. van Wees, Phys. Rev. B **62**, R4790 (2000).
[18] M. Popinciuc *et al.* (to be published).
[19] M. Brandsa and G. Dumpich, J. Appl. Phys. **98**, 014309 (2005).
[20] We note that an anisotropic g factor, similar to graphite and carbon nanotubes, can also be expected in graphene. However, our spin precession measurements we perform are not suited to detect such a weak anisotropy in the g factor. O. Chauvet, L. Forro, W. Bacsa, D. Ugarte, B. Doudin, and Walt A. de Heer, Phys. Rev. B **52**, R6963 (1995).
[21] K. I. Bolotin, K. J. Sikes, Z. Jiang, G. Fudenberg, J. Hone, P. Kim, and H. L. Stormer, arXiv:0802.2389v1.